Enhanced Electrocatalytic Nitrate-to-Ammonia Performance from Mott-Schottky Design to Induce Electron Redistribution

Ruikai Qi,[‡a] Qiuling Jiang,[‡b,d] Li Deng,[a] Xianqiang Yu,[a] Bingyan Shi,[a] Mengxiao Zhong,[c]* Ying Wang,[b]* Xiaofeng Lu[a]*

[a]Alan G. MacDiarmid Institute, College of Chemistry, Jilin University, Changchun 130012, P.R. China. E-mail: xflu@jlu.edu.cn

[b]State Key Laboratory of Rare Earth Resource Utilization, Changchun Institute of Applied Chemistry, Chinese Academy of Sciences, Changchun, 130022, China. Email: ywang_2012@ciac.ac.cn

[c]State Key Laboratory of Integrated Optoelectronics, Key Laboratory of Advanced Gas Sensors, Jilin Province, College of Electronic Science and Engineering, Jilin University, 2699 Qianjin Street, Changchun, 130012 P. R. China. Email: zhongmx@jlu.edu.cn

[d]School of Applied Chemistry and Engineering, University of Science and Technology of China, Hefei, 230026, China

[‡]These authors contributed equally to this work.

[†]Electronic supplementary information (ESI) available.

Keywords: Mott-Schottky effect, heterostructure, electrospinning, nitrate-to-ammonia

1. Experiment section

1.1 Chemicals

Poly(vinylpyrrolidone) (PVP, M_w=1300000 g mol^{-1}) was purchased from Thermo Scientific, indium nitrate hydrate ($In(NO_3)_3·4.5H_2O$) and cobalt nitrate hexahydrate ($Co(NO_3)_2·6H_2O$) were provided by Aladdin Chemistry Co., Ltd. Nafion solution was acquired from Shanghai Hesen Electric Co., Ltd. N,N-dimethylformamide (DMF) and ethanol were available from Sinopharm Chemical Reagent Co., Ltd.

1.2 Preparation of Co/In_2O_3

Firstly, of 0.239 g $Co(NO_3)_2·6H_2O$, 0.261 g of $In(NO_3)_3·4.5H_2O$ and 0.5 g of PVP were added into a mixture system consisting of 2.5 mL of ethanol and 2.5 mL of DMF to produce a uniformly mixed precursor solution. Then, the $Co(NO_3)_2/In(NO_3)_3$/PVP precursor was adopted for electrospinning under a voltage of 18 kV. Next, the precursor was heated to 450 °C in air with a heating rate of 2 °C for 2 h. Finally, after cooling to the room temperature, the collected product was named as Co_3O_4/In_2O_3–1 fibers. Subsequently, the obtained oxide fibers were placed in a tube furnace and reduced at 400°C with a heating rate of 2 °C for 4 h in a H_2/Ar atmosphere to obtain the product Co/In_2O_3–1. By contrast, the synthesis procedures for the preparation of other control samples are consistent with that to obtain Co/In_2O_3. Specifically, Co/In_2O_3–0.5 was obtained by varying the added amounts of 0.157 g of $Co(NO_3)_2·6H_2O$ and 0.343 g of $In(NO_3)_3·4.5H_2O$. Co/In_2O_3–2 was obtained by varying the added amounts of 0.323 g of $Co(NO_3)_2·6H_2O$ and 0.177 g of $In(NO_3)_3·4.5H_2O$. Co was obtained by varying the added amounts of 0.5 g of $Co(NO_3)_2·6H_2O$, and In_2O_3 was obtained by varying the added amounts of 0.5 g of $In(NO_3)_3·4.5H_2O$. The obtained In_2O_3 sample after H_2/Ar reduction treatment is defined as In_2O_3-H.

1.3 Electrochemical measurement

Electrochemical measurements were conducted using CHI 660E electrochemical workstation within an H–type electrolytic cell. Hg/HgO electrode was used as the reference electrode and Pt wire was used as counter electrode. The working electrode was prepared as follows: 4 mg of sample was dispersed in 980 μL ethanol and 20 μL Nafion mixture solution to form a uniform catalyst ink. Then, a certain amount of ink

was dropped on the surface of a carbon cloth electrode to attain a mass loading of 1 mg cm^{-2}. The anode and cathode chambers were filled with 1.0 M KOH solution (30 mL), followed by the introduction of 0.1 M KNO_3 into the cathode chamber for nitrate reduction testing. LSV curves were generated until a stable state occured with a potential range from –0.6 to –1.8 V relative to Hg/HgO. Unless otherwise specified, all the potentials are corrected relative to reversible hydrogen electrodes (RHE) (Figure S24, $E_{RHE}=E_{Hg/HgO}+0.93$ V). Chronoamperometric tests were conducted at different potentials for 1 h. The cycling stability test was conducted by filling the anode and cathode chambers with 1.0 M KOH solution (100 mL), and then introducing 0.1 M KNO_3 into the cathode chamber for nitrate reduction testing. The Mott–Schottky curve test was carried out in a three electrode system, with platinum wire as the counter electrode and Ag/AgCl as the reference electrode. In_2O_3–H loaded on a glassy carbon electrode with a loading amount of 1mg cm^{-2} was used as a working electrode and the electrolyte is 0.5 M $NaSO_4$. The aqueous Zn-NO_3^- battery was assembled using Co/In_2O_3–1 (1×1 cm^2, 1 mg cm^{-2}) as the cathode and Zn foil (1×1 cm^2) as the anode, 30 mL of 1 M KOH with 0.1 M KNO_3 as the cathode electrolyte, and 30 mL of 3 M KOH as the anode electrolyte.

1.4 Material Characterization

Field emission scanning electron microscopy (FESEM) was constructed using a FEI Nova NanoSEM and FEI Thermo measurement. Transmission electron microscopy (TEM) was conducted by JEM-2100 F, JEOL and high-resolution TEM (HRTEM, FEI Tecnai G2 F20). High-resolution transmission electron microscopy (HRTEM), elemental mapping and energy dispersive X-ray (EDX) spectroscopy were obtained by using a FEI Tecnai G2 F20 electron microscope. Inductively coupled plasma-optical emission spectrometry (ICP-OES) were using Agilent 725. X-ray photoelectron spectra (XPS) analysis was performed on Thermo Scientific Nexsa measurement. X-ray diffraction (XRD) patterns were obtained by PANalytical B.V and Rigaku DESKTOP. The model of the Fourier Transform Infrared (FTIR) spectrometer (Bruker) testing instrument is VECTOR22. Avance NEO NMR spectrometer (400 MHz) was employed to ascertain the origin of ammonia. Ultraviolet-visible diffuse reflectance spectra (UV-

vis DRS) were carried out through PerkinElmer Lambda 850, with $BaSO_4$ as a reference.

1.5 Determination of ion concentration.

The ultraviolet-visible (UV-vis) spectrophotometer was carried out to measure the ion concentration of the electrolyte following the test.

1.5.1 NO_3–N

A certain amount of electrolyte was removed from our electrolytic cell and diluted to a convenient 4 mL. Subsequently, 0.08 mL of 1 M HCl and 0.008 mL of 0.8 wt% amino sulfonic acid solution were added into the above solution. An UV-vis spectrophotometer was then employed to observe the absorption spectrum. This was followed by generating a calibration curve of absorbance concentration using several standard potassium nitrate solutions.

1.5.2 NO_2–N

An aqueous system consisting of *p*–aminobenzenesulfonamide (4 g), N-(1-Naphthyl) ethylenediamine dihydrochloride (0.2 g), ultrapure water (50 mL) and phosphoric acid (10 mL, ρ=1.70 g mL^{-1}) was employed as a colorimetric reagent. An amount of the electrolyte was diluted to 4 mL, then 0.1 mL of the afore-mentioned colorimetric reagent was added to the above solution and gently mixed. An UV-vis spectrophotometer was utilized to assess the absorption spectrum. The absorbance-concentration curve was calibrated using a series of standard potassium nitrite solutions.

1.5.3 NH_3–N

An amount of the electrolyte was diluted to 4 mL, then 0.1 mL of potassium sodium tartrate solution (ρ=500 g L^{-1}) was added to above solution. In the following, 0.1 mL of Nessler's reagent was injected into the mixture. A UV-vis spectrophotometer was utilized to provide the absorption spectrum. The absorbance-concentration curve was calibrated using a series of standard ammonium chloride solutions.

1.6 Isotope Labeling Experiments

1 M KOH and 0.1 M $K^{15}NO_3$ solution were employed as electrolyte. Following 1 h chronoamperometry test at –0.8 V *vs.* RHE, the electrolyte was removed and mixed with 0.08 mL of hexadeuterodimethyl sulfoxide (DMSO-d6) and 0.08 wt% of Maleic acid ($C_4H_4O_4$) for ^1H NMR (400 MHz) testing.

1.7 Calculation of the NH_3 yield rate and Faradaic efficiency

The NH_3 yield rate is calculated by the Eq.1

$$\text{Yield rate}_{NH_3} = \frac{c_{NH_3} \times V}{M_{NH_3} \times t \times S}$$

The NH_3 Faradaic efficiency is calculated by the Eq. 2:

$$\text{Faradaic efficiency}_{NH_3} = \frac{8 \times F \times c_{NH_3} \times V}{M_{NH_3} \times Q}$$

where c_{NH3} is the mass concentration of NH_3 (aq), V is the volume of electrolyte in the cathode compartment (30 mL or 100 mL), M_{NH3} is the molar mass of NH_3, t is the electrolysis time (1 h), S is the geometric area of working electrode (0.2 cm^2), c is the generated concentration of ammonia, F is the Faradaic constant (96485 C mol^{-1}), Q is the total charge passing the electrode.

2. Computational methods

Vienna Ab initio Simulation Package (VASP) was used to carry out the spin-polarized density functional theory (DFT) calculation.[1] The generalized gradient approximation (GGA) with Perdew-Burke-Ernzerhof (PBE) exchange-correlation functional was carried out for electron correlation.[2] The valence electron wave functions were expanded in a plane wave basis set with an energy cutoff of 400 eV, and the core electrons were represented by the projector augmented-wave (PAW) method.[3] For geometry optimization, a 3×3×1 k-point grid was used, while electronic structure calculations was opted for a denser 5×5×1 grid, both following the Monkhorst-Pack scheme. The force and energy convergence criteria were set to 0.05 eV/Å and 10^{-5} eV. A Van der Waals correction was applied using the DFT-D3 method.[4] For pristine Co and the In_2O_3, (111) surface for Co and (211) surface for In_2O_3 were chosen, and three-layer slabs were constructed with 2×2 surface unit cells. To model the Co/In_2O_3 structure, a Co cluster consisting of 26 atoms was gently attached to the In_2O_3 (211) surface. All the slabs were separated by a 15 Å vacuum space in the Z-direction to avoid periodic interactions. The corresponding reaction free energies (ΔG) were calculated using the computational hydrogen electrode (CHE) model:[5]

$$\Delta G = \Delta E + \Delta ZPE - T\Delta S$$

where ΔE is the energy difference between the products and reactants, ΔZPE is the zero-

point energy correction, and $T\Delta S$ is the entropy change.

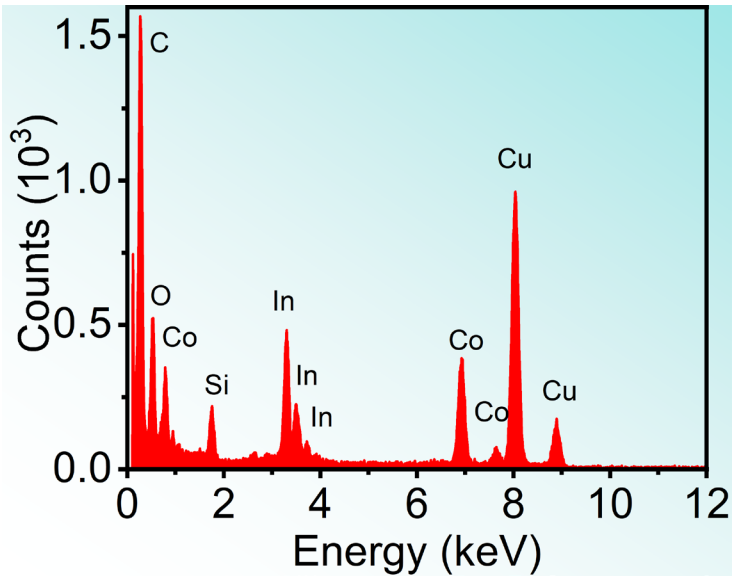

Figure S1. EDX spectrum of Co/In_2O_3–1 sample.

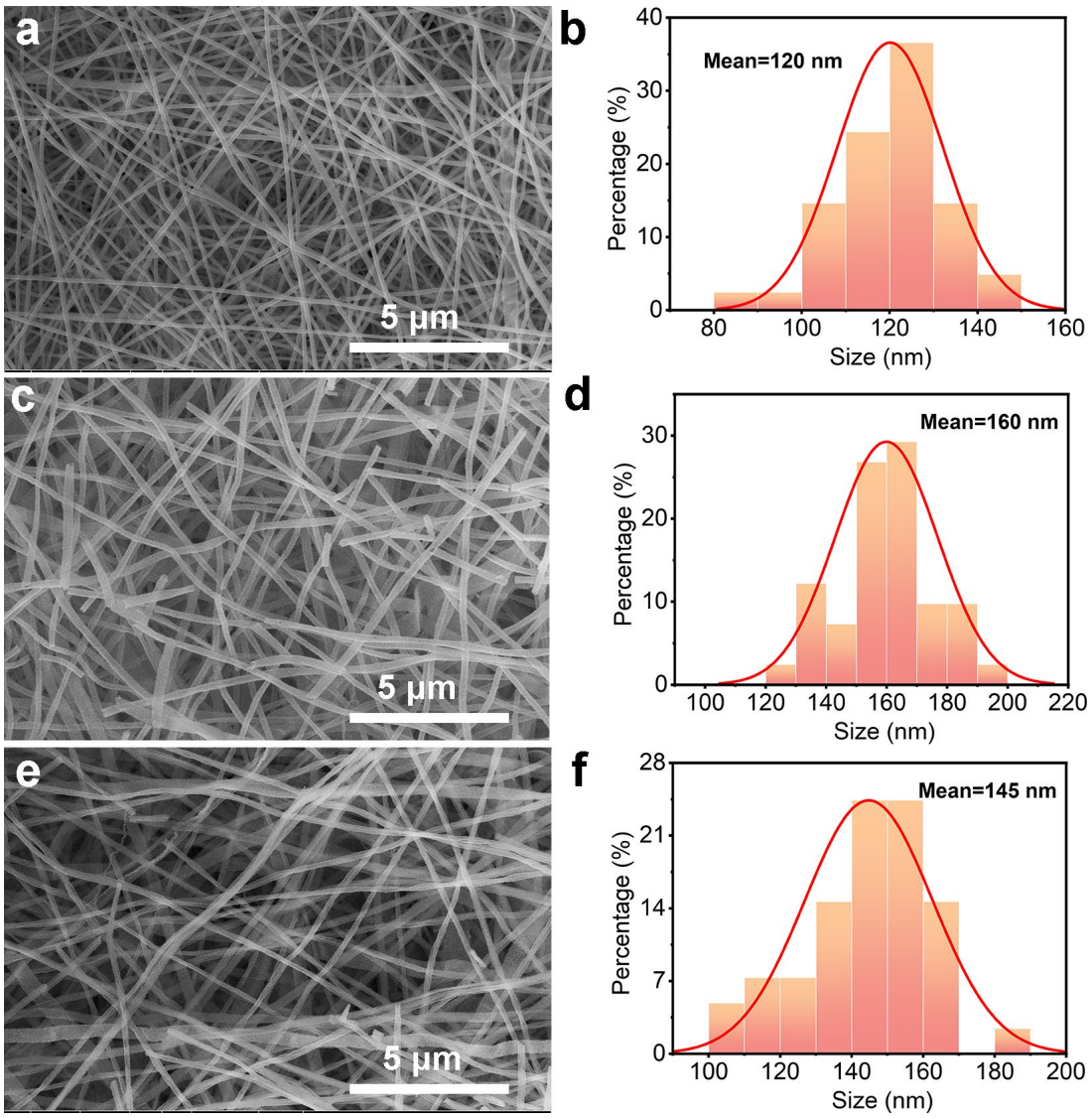

Figure S2. (a, c, e) SEM images and (b, d, f) diameter distribution of (a, b) In_2O_3, (c, d) Co_3O_4/In_2O_3–0.5 and (e, f) Co_3O_4/In_2O_3–2.

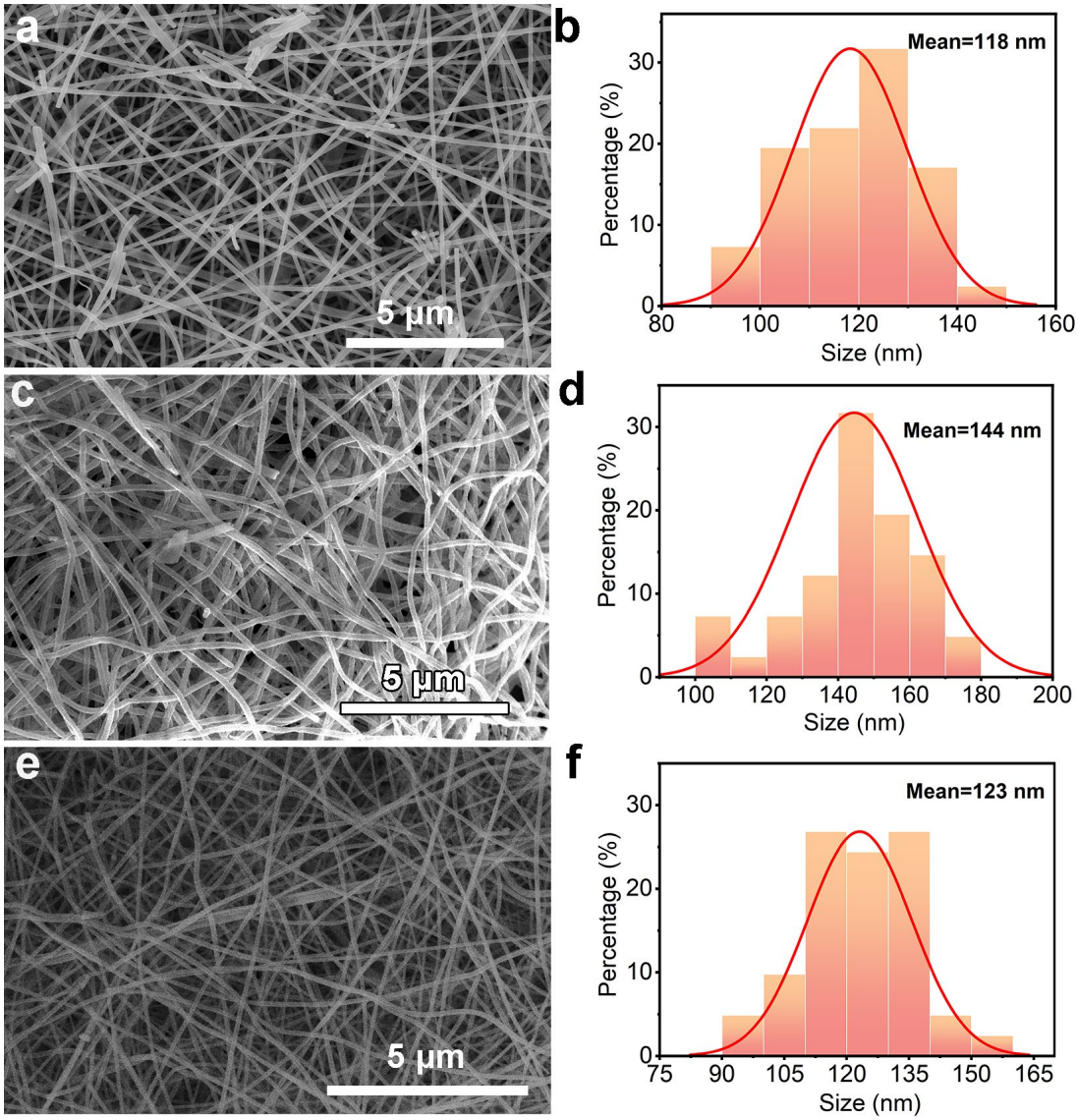

Figure S3. (a, c, e) SEM images and (b, d, f) diameter distribution of (a, b) In_2O_3–H, (c, d) Co/In_2O_3–0.5 and (e, f) Co/In_2O_3–2.

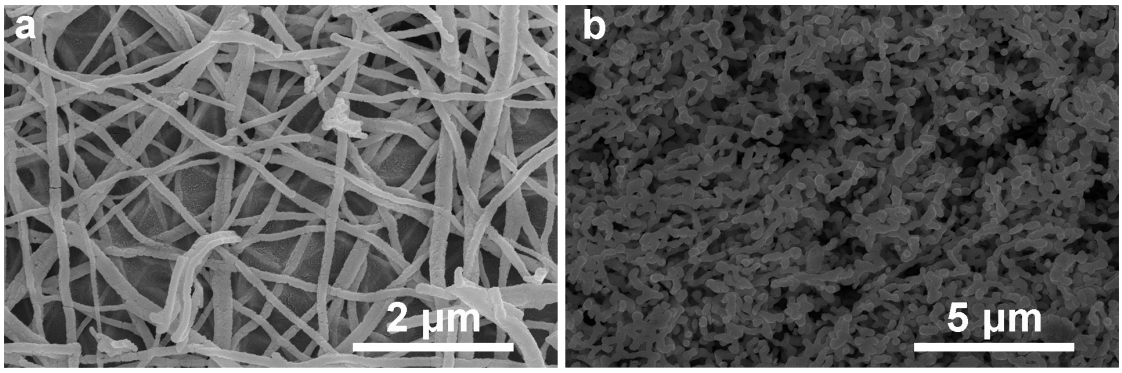

Figure S4. SEM images of (a) Co_3O_4 and (b) Co.

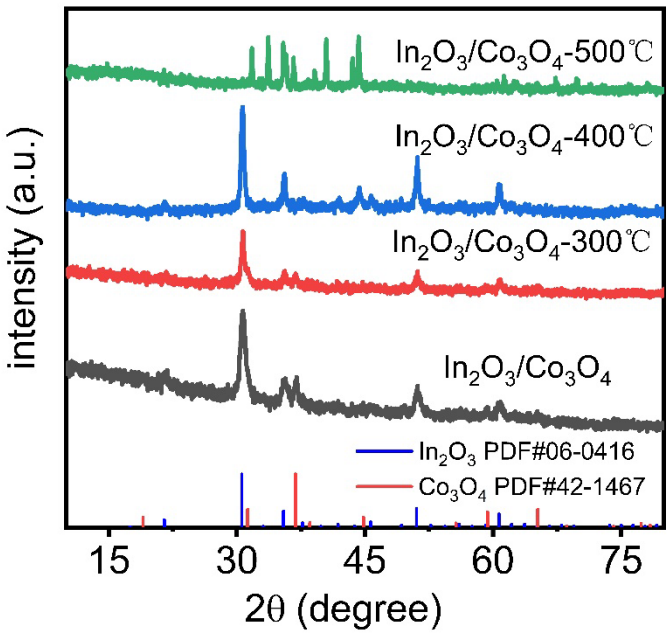

Figure S5. XRD pattern of Co_3O_4/In_2O_3–1 under different reduction temperature in H_2/Ar atmospheres.

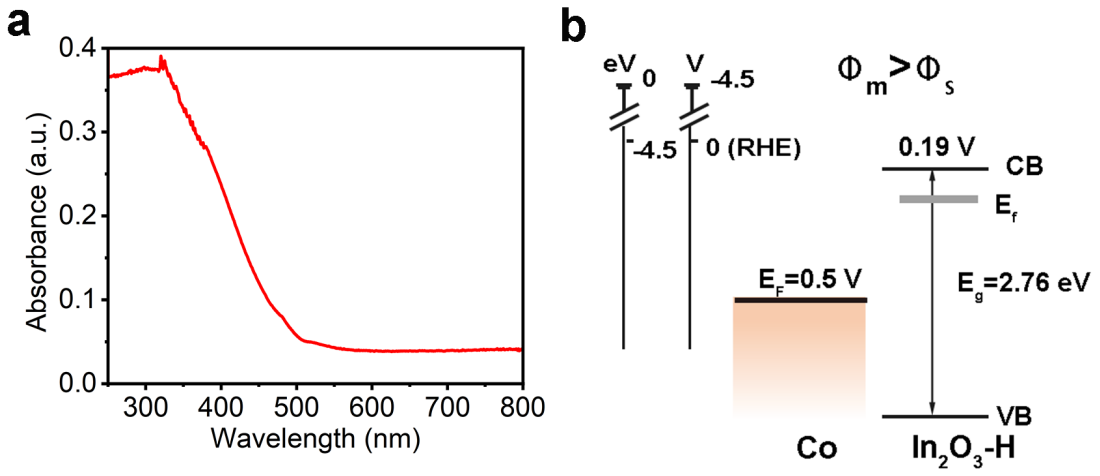

Figure S6. (a) UV–vis absorbance spectra of the In_2O_3 colloidal dispersions, revealing the significant absorbance in the UV region. (b) Proposed band diagrams of Co/In_2O_3 before the Mott–Schottky contact.

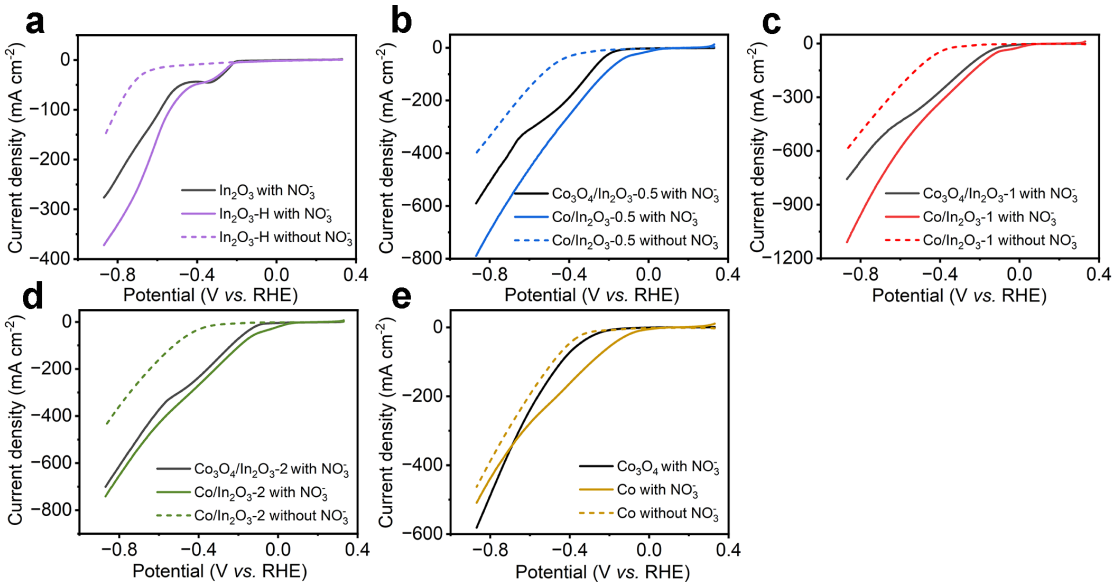

Figure S7. LSV curves of (a) In_2O_3–H, (b) Co/In_2O_3–0.5, (c) Co/In_2O_3–1, (d) Co/In_2O_3–2 and (e) Co in 1 M KOH with and without 0.1 M KNO_3. Electrochemical performance was performed without *iR*–correction.

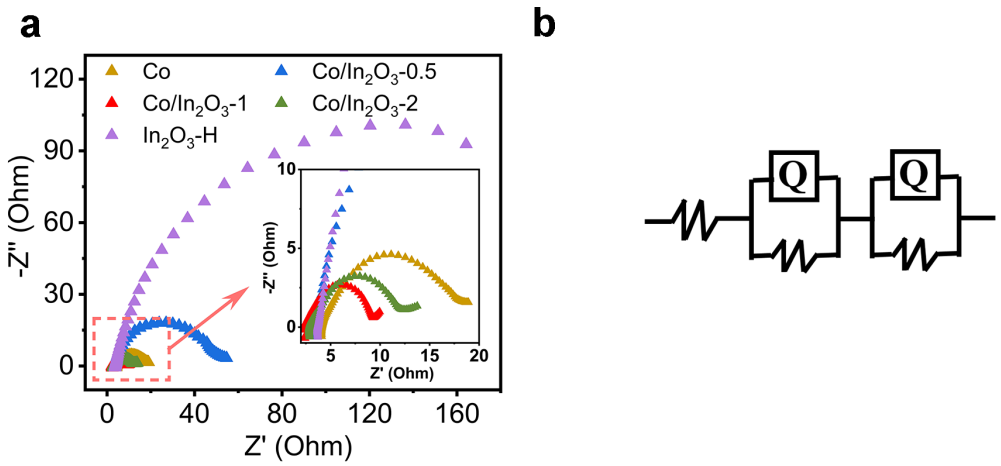

Figure S8. (a) The Nyquist plots of different catalysts at the potential of –1.0 V *vs.* Hg/HgO electrode. (b) The fitted equivalent for the Nyquist plots.

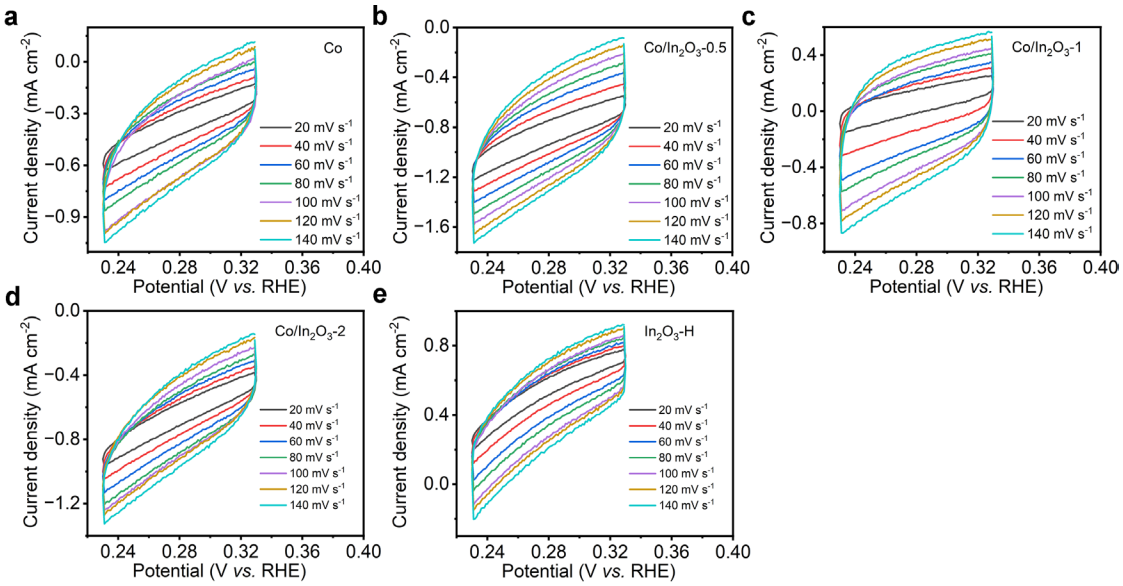

Figure S9. Cyclic voltammograms (CV) for the determination of the double-layer capacitance of different samples. (a) Co, (b) Co/In_2O_3–0.5, (c) Co/In_2O_3–1, Co/In_2O_3–2 and (d) In_2O_3–H.

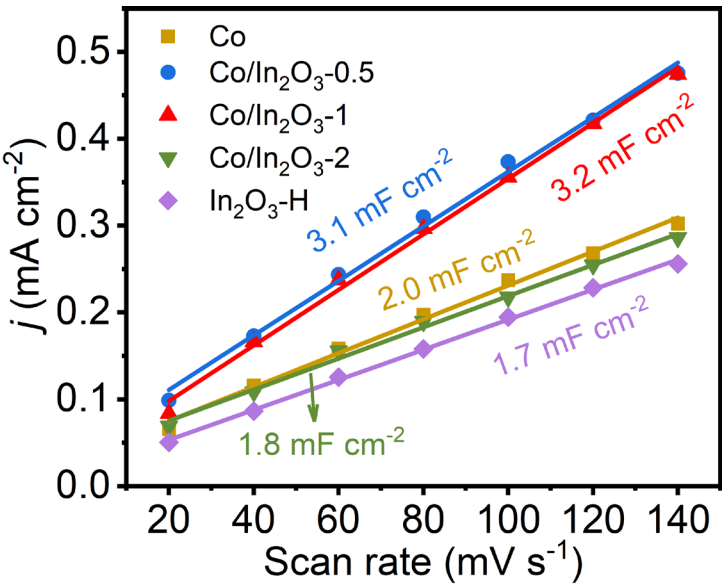

Figure S10. The capacitive current density ($j = (j_a - j_c)/2$) at different scan rates related to the C_{dl} of different catalysts.

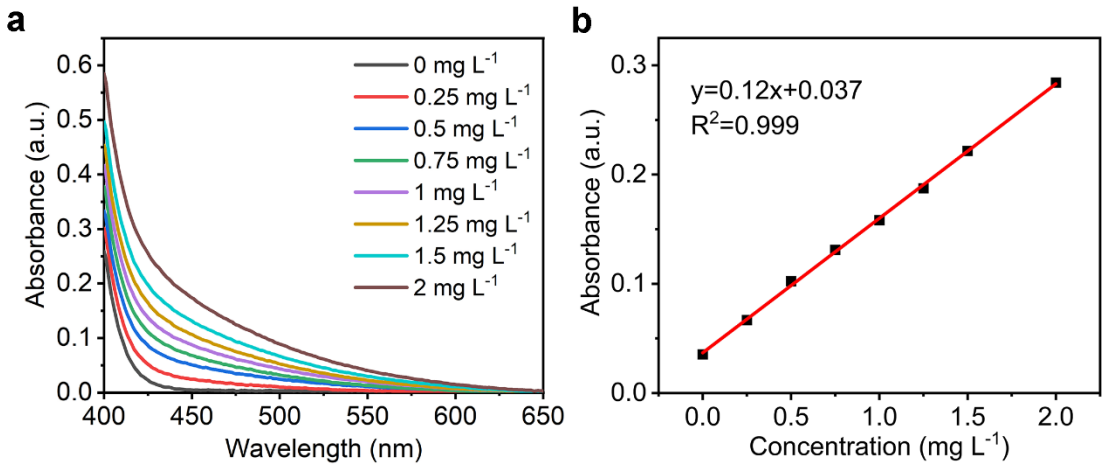

Figure S11. (a) The ultraviolet absorption and (b) concentration-absorbance calibration curve of NH_3–N.

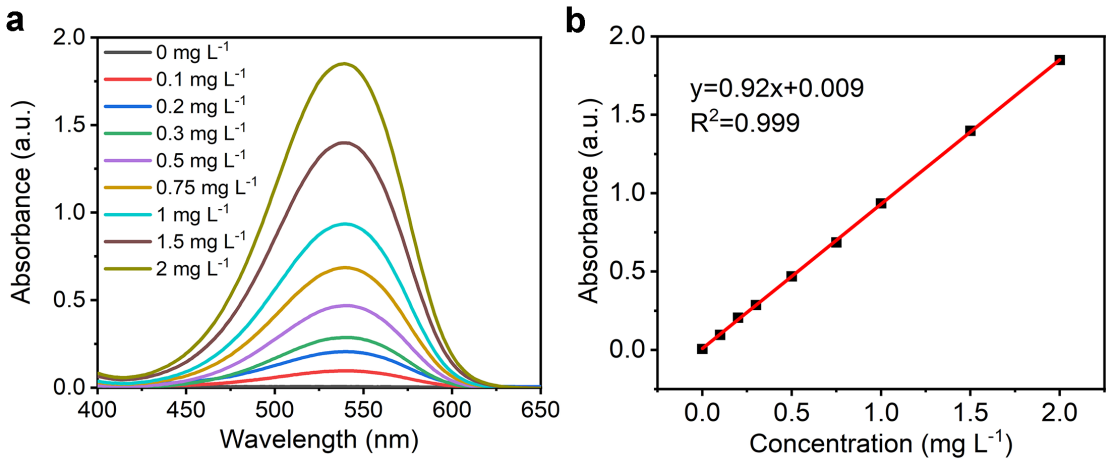

Figure S12. (a) The ultraviolet absorption and (b) concentration-absorbance calibration curve of NO_2^-–N.

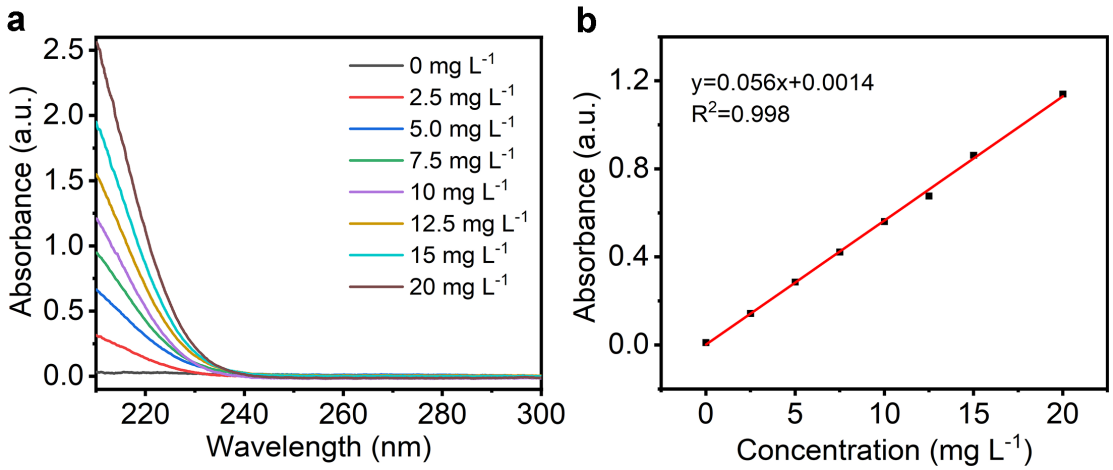

Figure S13. (a) The ultraviolet absorption and (b) concentration-absorbance calibration curve of NO_3^-–N.

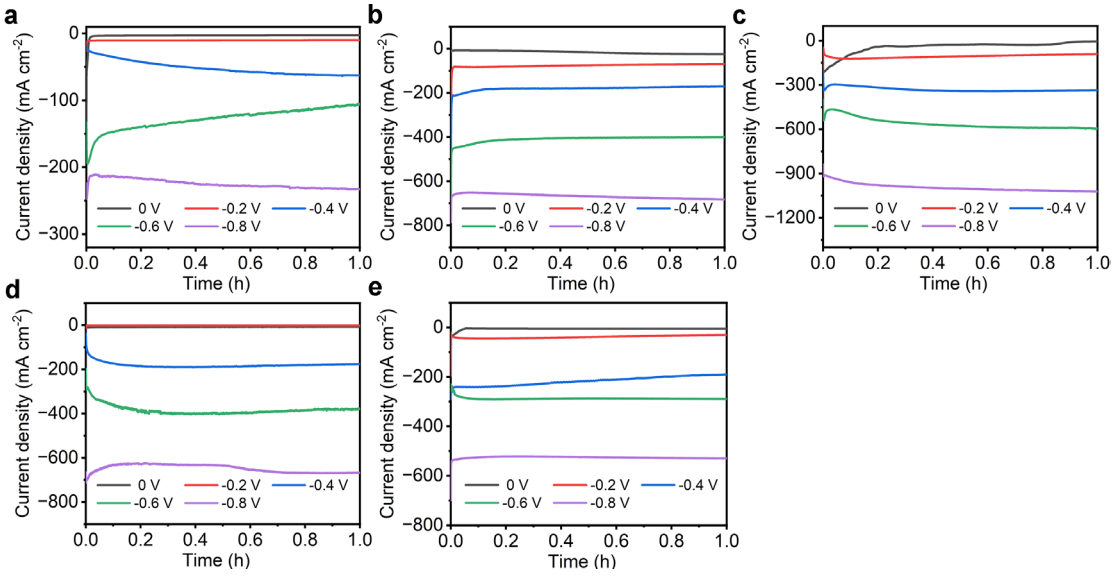

Figure S14. Chronoamperometry curves at different potentials for 1 h in 1.0 M KOH and 0.1 M KNO_3 by using varied electrocatalysts: (a) In_2O_3–H, (b) Co/In_2O_3–0.5, (c) Co/In_2O_3–1, (d) Co/In_2O_3–2 and (e) Co.

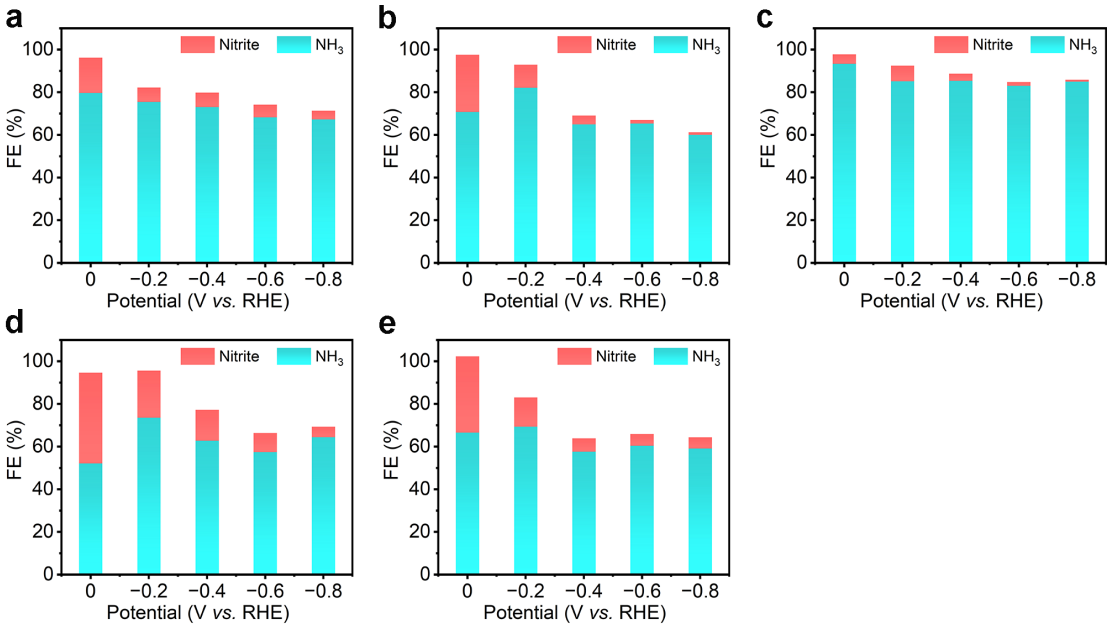

Figure S15. Product analysis at different potentials with varied electrocatalysts: (a) In_2O_3–H, (b) Co/In_2O_3–0.5, (c) Co/In_2O_3–1, (d) Co/In_2O_3–2 and (e) Co.

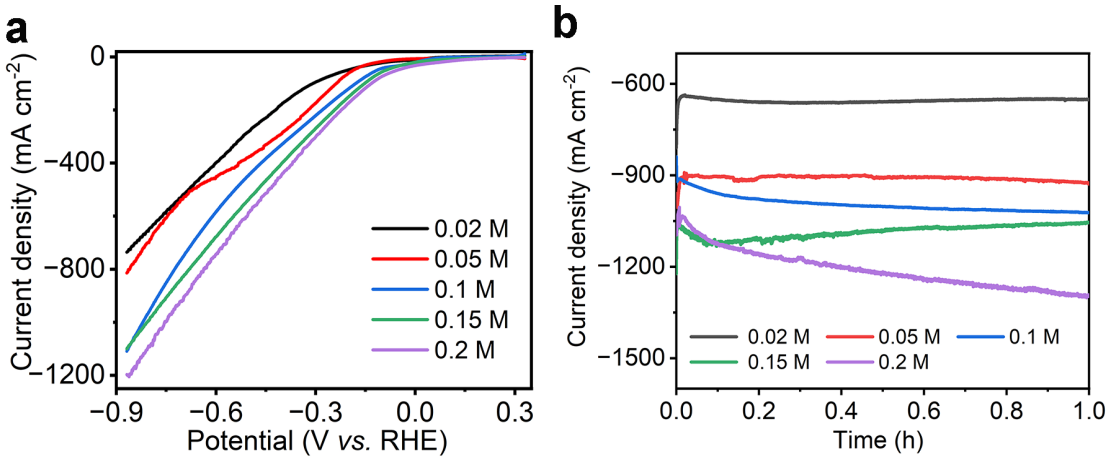

Figure S16. (a) LSV plots of Co/In_2O_3–1 for nitrate reduction with various concentration of KNO_3 ranging from 0.02 to 0.2 M without *iR* correction. (b) Chronoamperometry curves of Co/In_2O_3–1 under different concentration of KNO_3 at the potential of –0.8 V.

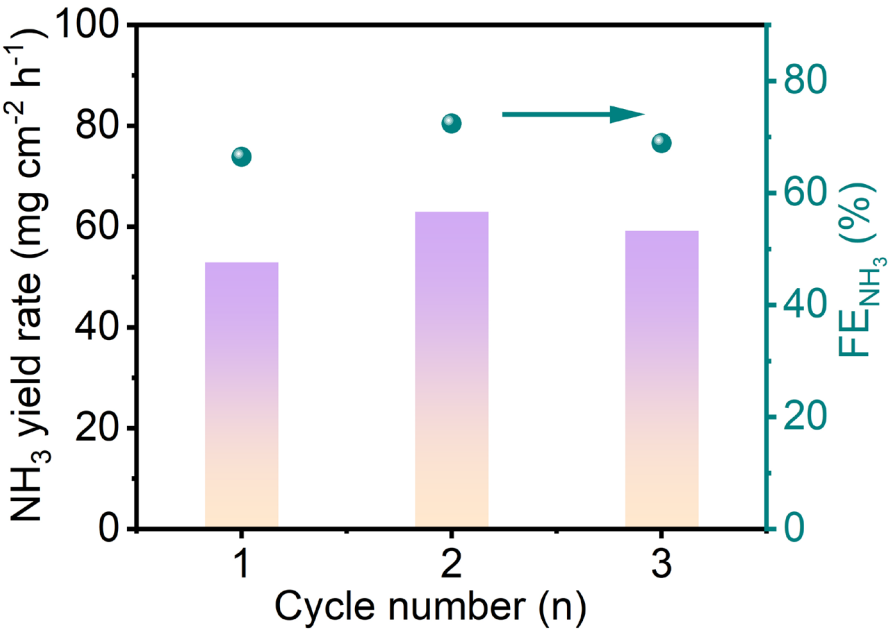

Figure S17. NH_3 FEs and yield rate of NH_3 after each cycle.

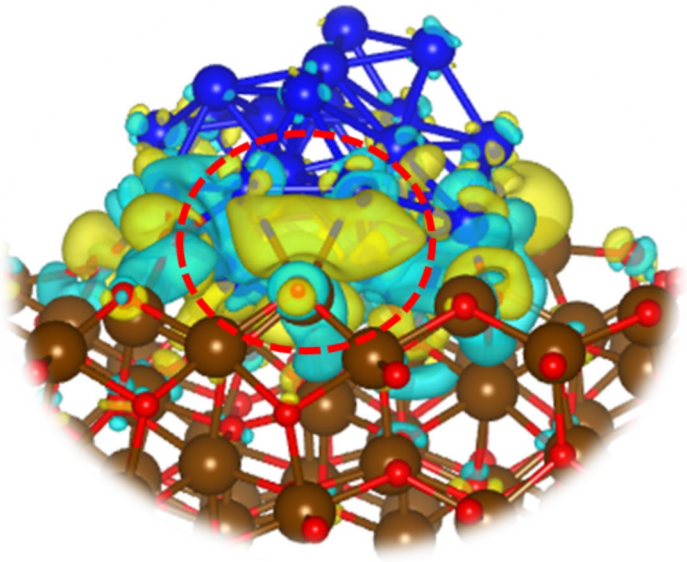

Figure S18. The charge density difference of Co/In_2O_3.

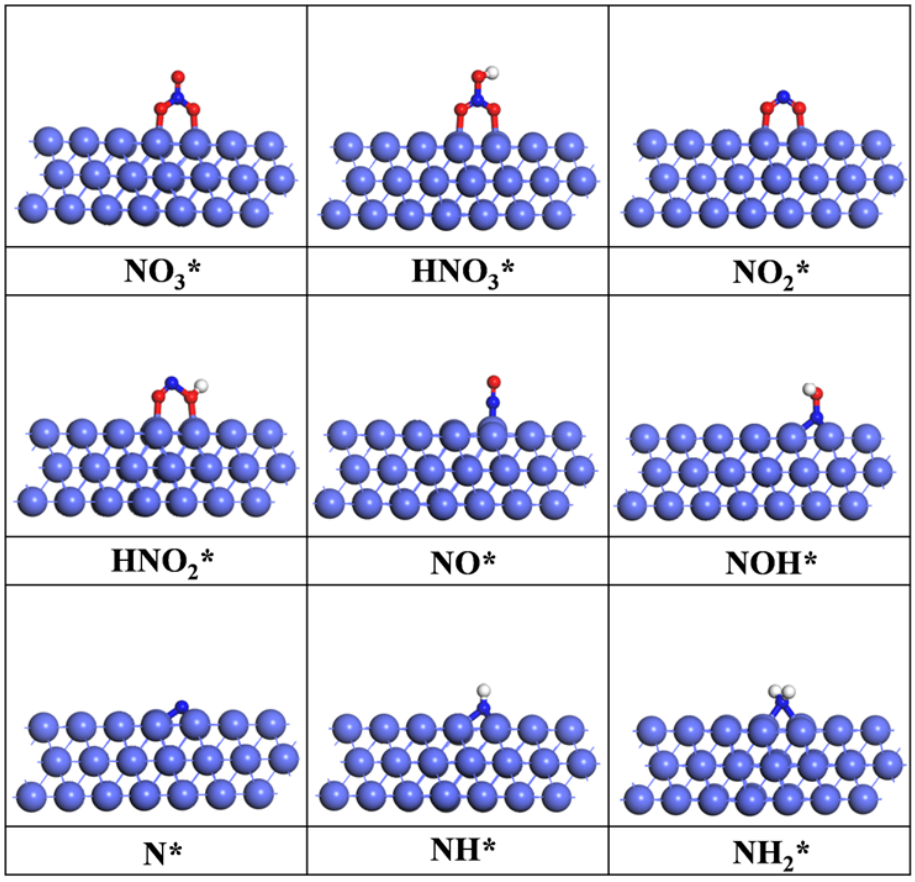

Figure S19. Optimized geometries of reaction intermediates on Co (111) in the most favorable reaction pathway. Red spheres depict oxygen atoms, light blue spheres depict cobalt atoms, dark blue spheres depict nitrogen atoms, and white spheres depict hydrogen atoms.

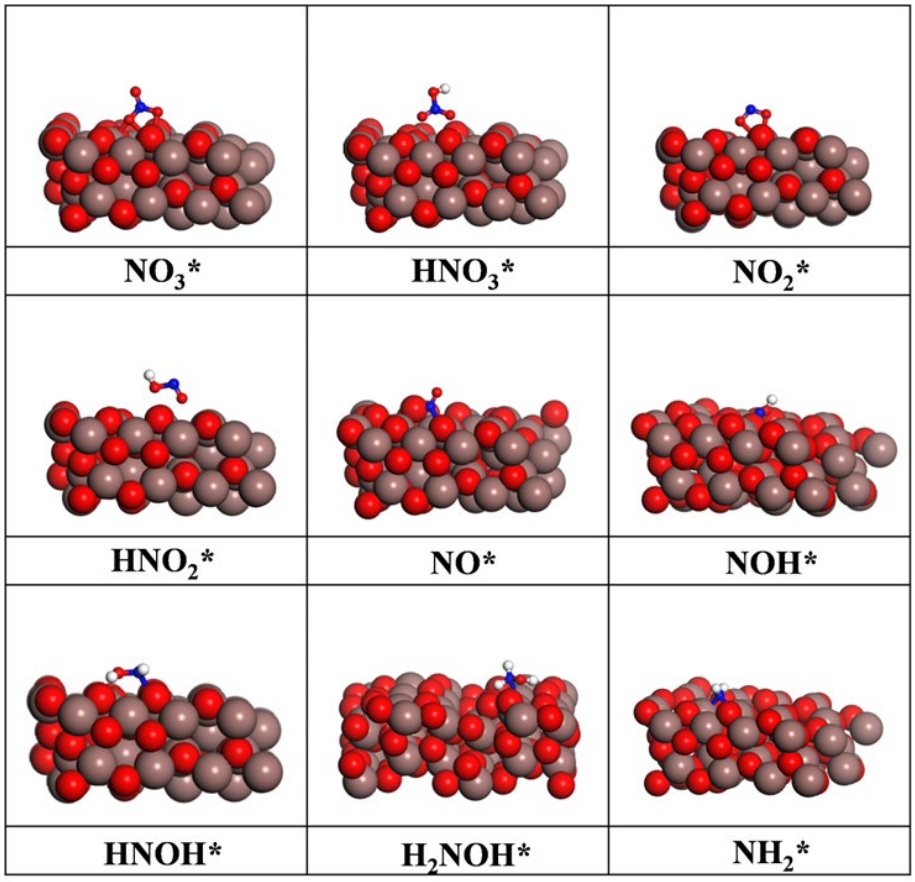

Figure S20. Optimized geometries of reaction intermediates on In_2O_3 (211) in the most favorable reaction pathway. Red spheres depict oxygen atoms, dark brown spheres depict indium atoms, dark blue spheres depict nitrogen atoms, and white spheres depict hydrogen atoms.

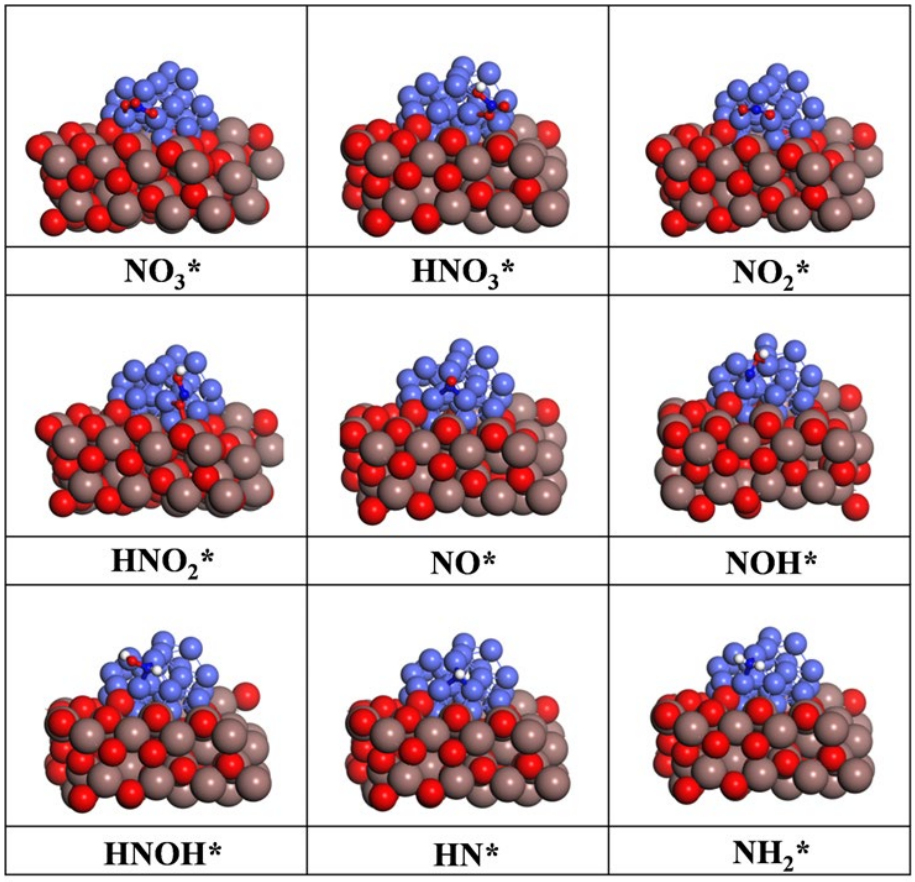

Figure S21. Optimized geometries of reaction intermediates on Co/In_2O_3 in the most favorable reaction pathway. Red spheres depict oxygen atoms, dark brown spheres depict indium atoms, light blue spheres depict cobalt atoms, dark blue spheres depict nitrogen atoms, and white spheres depict hydrogen atoms.

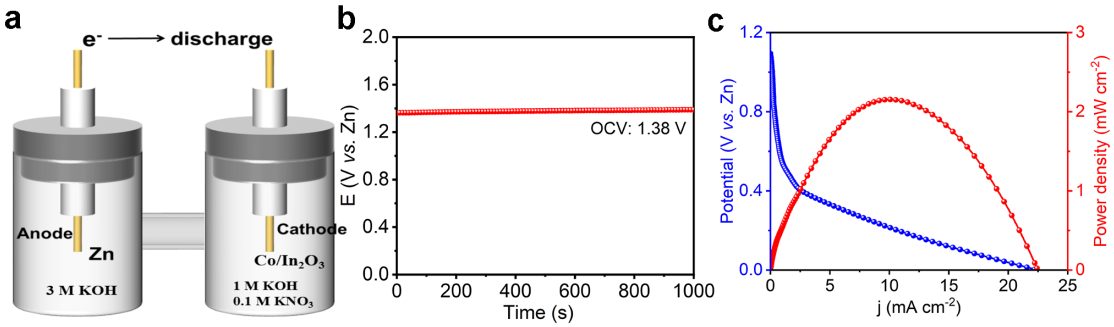

Figure S22. (a) Schematic illustration of the aqueous Zn-NO_3^- battery. (b) Open-circuit voltage, and (c) discharging polarization curves and corresponding powder density curves of Zn-NO_3^- battery.

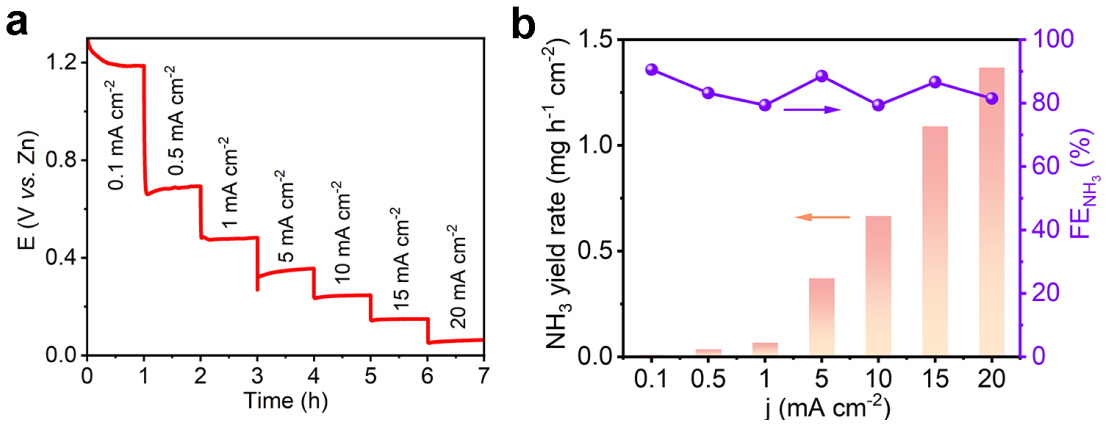

Figure S23. (a) Discharging tests of Co/In_2O_3-1 at various current densities. (b) NH_3 FEs and yield rate at various current densities.

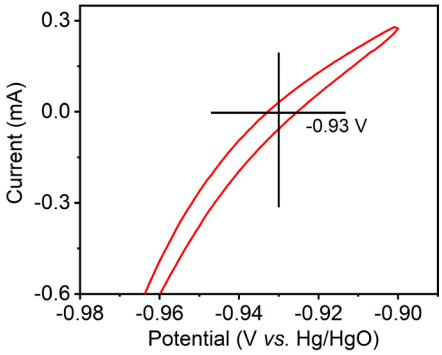

Figure S24. CV curves of the calibration of the Hg/HgO electrode at the scan rate of 1 mV s^{-1} in 1 M KOH solution.

Table S1. The ratio of Co to In in the as-synthesized materials measured by ICP-OES.

Sample	Co/In_2O_3-0.5	Co/In_2O_3-1	Co/In_2O_3-2
Co:In molar ratio	0.4604	0.9999	2.0982

Table S2. Comparison of the NH_3 yield rate of Co/In_2O_3-1 with other reported electrocatalysts.

Catalysts	Electrolyte	NH_3 yield rate	Reference
Co/In_2O_3-1	1 M KOH 0.1 M KNO_3	70.1 mg cm^{-2} h^{-1} at -0.8 V *vs.* RHE	This work
$NiCo_2O_4$/CC	1 M KOH 0.1 M KNO_3	0.9732 mmol cm^{-2} h^{-1} -0.3 V *vs.* RHE	*Small*., 2022, **18**, e2106961.
Co-B@CoO_x	0.5 M Na_2SO_4 100 ppm NO_3^-	0.96 mg h^{-1} cm^{-2} −0.75 V *vs.* RHE	*Energy Environ. Sci*., 2024,**17**, 2908-2920
FeCoNiAlTi	0.2 M K_2SO_4 50 mM KNO_3	0.36 mg h^{-1} cm^{-2} -0.5 V *vs.* RHE	*Angew. Chem. Int. Ed*., 2024, **63**, e202407589
$Cu_{50}Co_{50}$ nanosheet	0.1 M NO_3^- 1 M KOH	4.83 mmol h^{-1} cm^{-2} -0.2 V *vs.* RHE	*Nat. Commun*., 2022, **13**, *7899*
CoCuSP	0.1 M NO_3^- 1 M KOH	1.17 mmol cm^{-2} h^{-1} -0.175 V *vs.* RHE	*Nat. Commun*., 2022 **13**, 1129
MAT-CoNi/CF	0.1 M NO_3^- 1 M KOH	1.476 mmol cm^{-2} h^{-1} -0.15 V *vs.* RHE	*Adv. Mater*., 2024, **36**, 2404774
CoP NAs/CFC	0.1 M $NaNO_3$ 1 M NaOH	9.56 mol h^{-1} m^{-2} -0.3 V *vs.* RHE	*Energy Environ. Sci*., 2022, **15**, 760
Co-NAs	1 M KOH 0.1 M KNO_3	4.16 mmol h^{-1} cm^{-2} -0.14 V *vs.* RHE	*Adv. Sci*., 2021, **8**, 2004523
Co_2AlO_4 nanoarray	0.1 M $NaNO_3$ 0.1 M PBS	6.2 mg h^{-1} cm^{-2} -0.70 V *vs.* RHE	*Chem. Eng. J*., 2022, **435**, 135104
P-Cu/$Co(OH)_2$	1 M KOH 0.1 M KNO_3	42.63 mg h^{-1} cm^{-2} -0.40 V *vs.* RHE	*Adv. Mater.* 2024, 2408680
FePc/TiO_2-2	1 M KOH 0.4 M KNO_3	17.4 mg h^{-1} cm^{-2} -0.75 V *vs.* RHE	*Nat. Commun.* 2023, **14**, 8036
Cu@ZnO NWA	0.1 M KOH 0.1 M KNO_3	5.608 mg h^{-1} cm^{-2} -0.6 V *vs.* RHE	*ACS Catal.* 2024, **14**, 5911

Ni_3B@$NiB_{2.74}$	0.1 M KOH 0.1 M KNO_3	3.3711 mg h^{-1} cm^{-2} -0.2 V *vs.* RHE	*Angew. Chem. Int. Ed.* 2021, **60**, 14131
$(Co_{0.83}Ni_{0.16})_2Fe$	1 M KOH 0.1 M KNO_3	50.15 mg h^{-1} cm^{-2} -0.42 V *vs.* RHE	*Angew. Chem. Int. Ed.* 2024, **63**, e202400428
RuO_x/Pd	1 M KOH 0.1 M KNO_3	23.46 mg h^{-1} cm^{-2} -0.5 V *vs.* RHE	*ACS Nano* 2023, **17**, 1081

References

1 J. Hafner, *J. Comput. Chem*., 2008, **29**, 2039.

2 J. Perdew, K. Burke, and M. Ernzerhof, *Phys. Rev. Lett*., 1996, **77**, 3865.

3 B. Hammer, L. B. Hansen and J. K. Nørskov, *Phys. Rev. B*., 1999, **59***,* 7413.

4 S. Grimme, *J. Comput. Chem*., 2006, **27**, 1787.

5 J. K. Nørskov, J. Rossmeisl. A. Logadottir, L. Lindqvist, J. R. Kitchin, T. Bligaard, and H. Jónsson, *J. Phys. Chem. B*., 2004, **108**, 17886.